Nano Res (2010) 3: 264–270
DOI 10.1007/s12274-010-1029-x
Research Article

In Situ Etching for Total Control Over Axial and Radial Nanowire Growth

Magnus T. Borgström[1] (✉), Jesper Wallentin[1], Johanna Trägårdh[1,§], Peter Ramvall[1], Martin Ek[2], L. Reine Wallenberg[2], Lars Samuelson[1], and Knut Deppert[1]

[1] Solid State Physics, Lund University, Box 118, S-221 00, Lund, Sweden
[2] Polymer & Materials Chemistry/nCHREM, Lund University, S-22100 Lund, Sweden
[§] Present Address: H. H. Wills Physics Laboratory, University of Bristol, Tyndall Avenue, Bristol BS8 1TL, United Kingdom

Received: 11 January 2010 / Revised: 7 February 2010 / Accepted: 7 February 2010

ABSTRACT

We report a method using *in situ* etching to decouple the axial from the radial nanowire growth pathway, independent of other growth parameters. Thereby a wide range of growth parameters can be explored to improve the nanowire properties without concern of tapering or excess structural defects formed during radial growth. We demonstrate the method using etching by HCl during InP nanowire growth. The improved crystal quality of etched nanowires is indicated by strongly enhanced photoluminescence as compared to reference nanowires obtained without etching.

KEYWORDS

MOVPE, nanowire growth, *in situ* etching, photoluminescence

1. Introduction

Recently nanowires (NWs) have attracted attention as one of the most promising ways to combine high-performance Ⅲ–Ⅴ materials with new functionality [1–4] and existing Si technology [5, 6]. An unintentional NW shell can harm device functionality by short circuiting axially designed components and by becoming a surrounding and competing recombination center [7] for charge carriers. Only by taking full control over radial growth can NWs be part of the future architecture for electronic devices. In order to promote axial in favor of radial NW growth, low growth temperature [8–10] and high supersaturation [11, 12] are typically used. The general trend in crystal growth however, is that such parameter settings lead to poor quality materials [13, 14]. Especially in metalorganic vapor phase epitaxy (MOVPE), a low growth temperature may lead to excess amphoteric carbon incorporation due to incomplete pyrolysis of the metalorganic precursors [14, 15]. The use of a high Ⅴ/Ⅲ ratio can lead to improved crystal layer quality and reduced carbon incorporation [16] as hydrogen radicals from decomposing group Ⅴ species eliminate group Ⅲ methyl groups by methane formation. For Ⅲ–Ⅴ semiconductor NWs however, there is only a narrow Ⅴ/Ⅲ parameter space resulting in growth of morphologically non-tapered NWs [17, 18].

We show here that *in situ* etching by use of HCl [19, 20] can prevent radial growth, despite growth conditions which would otherwise lead to strong

Address correspondence to magnus.borgstrom@ftf.lth.se

tapering. This allows total control over the design and growth of axially defined NW materials. Growth parameters can be fully optimized with respect to materials and device quality without concern of tapering issues. We find that crystal defects which are incorporated during uncontrolled radial growth can be completely removed by using HCl, and photoluminescence (PL) characterisation indicates that HCl diminishes carbon incorporation.

2. Experimental

Samples were prepared by depositing 80 nm diameter Au particles on a (111)B InP substrate via an aerosol technique [21] resulting in randomly distributed monodisperse particles with a homogeneous density of 5×10^7 cm^{-2}. The particle assisted NW growth was performed by use of a low-pressure (100 mbar) MOVPE system. Trimethylindium (TMI), and phosphine (PH_3) were used as precursors, and hydrogen chloride (HCl) as an etching agent in a total flow of 6.0 L/min using hydrogen (H_2) as carrier gas. The PH_3 and TMI molar fractions (χ_{PH_3}, χ_{TMI}) were set to $\chi_{PH_3} = 6.25 \times 10^{-3}$ and $\chi_{TMI} = 3.5 \times 10^{-6}$. Prior to growth, the samples were heated to 550 °C under a PH_3/H_2 gas mixture for 10 min in order to desorb any surface oxides. The reactor temperature was then reduced to a growth temperature of 450 °C, a regime where strong temperature-activated growth leading to tapering is expected. NW growth was initiated by adding TMI to the flow. HCl was added to the flow after a 15 s nucleation step, since the Au particles otherwise broke up into smaller particles. The HCl molar fraction was varied between 0 and 6.0×10^{-5} for growth of the NWs. Growth was terminated by switching off TMI and HCl simultaneously, and the samples were cooled down to room temperature under a mixture of PH_3 and H_2. Scanning electron microscopy (SEM) was used to characterize the NW morphology. Ten NWs from three different locations on each sample were evaluated for each data point.

Samples were prepared for high-resolution transmission electron microscopy (HRTEM) by direct transfer of the NWs to a Cu grid with a lacey carbon film by gently pressing the grid onto the substrate. Three types of NWs (prepared with $\chi_{HCl} = 0$, 1.0×10^{-5}, and 3.3×10^{-5}) were characterized by HRTEM. For each sample, images were recorded on the [110] zone axis in sequence along the length of a few NWs. The images were then Fourier filtered in order to enable separation of the contributions from zinc blende (ZB) and wurtzite (WZ) areas. For WZ the (0001) and the $(\bar{1}100)$ reflections were used whereas the (002) and $(\bar{1}\bar{1}1)$ reflections from each twin were used for ZB.

PL measurements were performed at a temperature of about 5 K. The NWs were broken off from the InP substrate and spread out on a metal covered surface. The NW under study was evenly illuminated throughout its length using a continuous wave (CW) laser emitting at 532 nm. The PL was collected by an optical microscope, dispersed through a spectrometer and detected by a thermoelectrically cooled charge coupled device (CCD) camera. At least five NWs per sample were studied.

3. Results and discussion

Figure 1 shows SEM images of InP NWs and the effect on the NW morphology of using different molar fractions of HCl, χ_{HCl}, during growth. Figure 1(a) shows a reference NW grown intentionally with parameters which give strong tapering when HCl is not present. The rough InP(111)B substrate surface indicates competing InP surface growth, which at these temperatures occurs below the temperature necessary for two-dimensional layer-by-layer growth [13]. By increasing χ_{HCl} in the flow, the NW tapering gradually decreases and the InP substrate roughness diminishes Figs. 1(b) and 1(c). The insets in Fig. 1 illustrate schematically the detrimental effect of a non-intentionally grown shell on a hypothetical axially defined NW structure based on heterostructures or doping. Note that in this paper we present data from *in situ* etching of a single undoped NW material only.

To assess the effect of *in situ* use of χ_{HCl} during NW growth we evaluated the NW length, NW volume, and the ratio between the bottom and top NW diameter (D_b/D_t) as a function of χ_{HCl} by SEM. The data are shown in Fig. 2. Figure 2(a) shows the effect of HCl on NW tapering. The ratio between the NW bottom and top diameter decreases linearly with χ_{HCl}, until radial growth is fully impeded ($D_b/D_t = 1$) for $\chi_{HCl} > 2.5 \times 10^{-5}$.

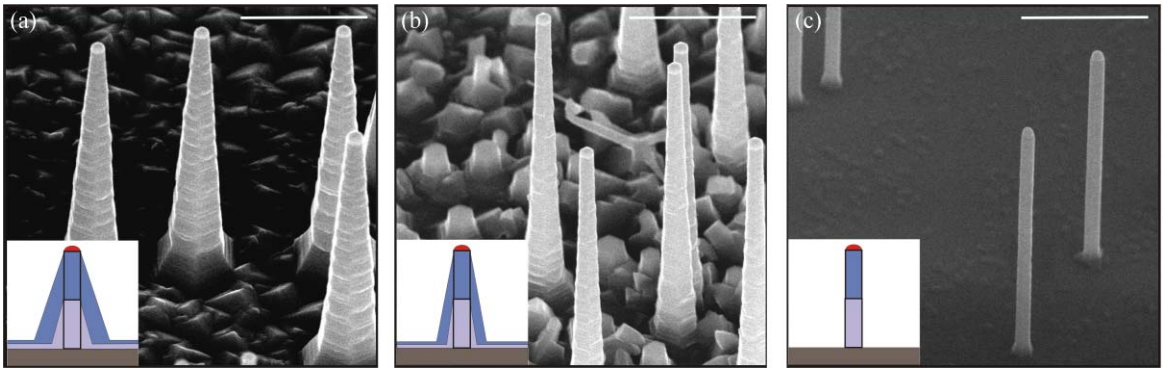

Figure 1 Scanning electron microscope images of *in situ* etched InP NWs. The 80 nm InP NWs were grown at 450 °C with different amounts of HCl in the gas phase: (a) reference InP NW, $\chi_{HCl} = 0$; (b) $\chi_{HCl} = 1.7 \times 10^{-5}$; (c) $\chi_{HCl} = 2.9 \times 10^{-5}$. The images are recorded at the same magnification and at an angle of 45° towards the normal to the substrate. The scale bars represent 1 μm. The insets are schematic illustrations of a hypothetical axially defined NW component with device functionality sensitive to tapering

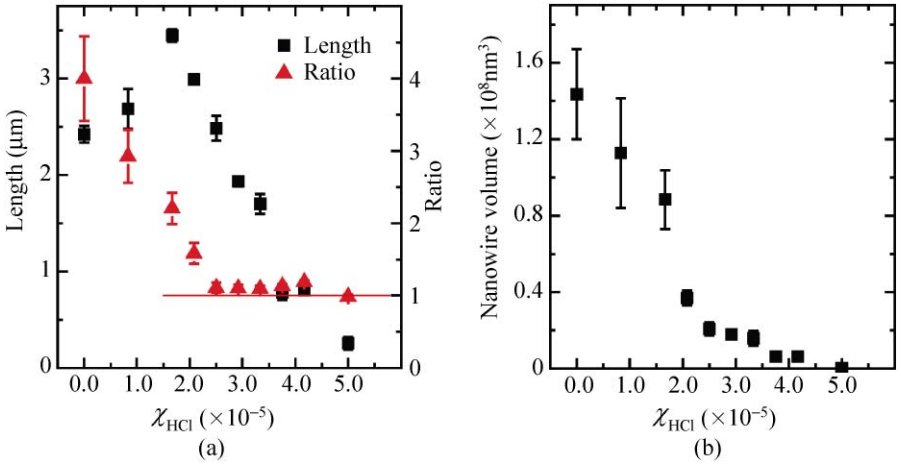

Figure 2 Effect of HCl on InP nanowire length, tapering, and volume. (a) The NW length is represented by squares, and the ratio between the bottom and top NW diameter (D_b/D_t) by triangles. The line is a guideline for the eye. (b) The NW volume evaluated by approximating the NW as a truncated cone. Error bars represent the standard deviation

The lengths of the reference NWs ($\chi_{HCl} = 0$) are about 2.5 μm. For values of χ_{HCl} up to 1.5×10^{-5} we observe an increase in the NW length (up to 3.5 μm) with increasing χ_{HCl}. For $\chi_{HCl} > 1.5 \times 10^{-5}$ the trend is reversed and a seemingly linear decrease of the NW length with increasing χ_{HCl} occurs. At $\chi_{HCl} = 6.0 \times 10^{-5}$ no NWs could be observed. Interestingly, even though the NW length decreases for $\chi_{HCl} > 2.5 \times 10^{-5}$, the NW diameter does not decrease further. This is a technically important regime, necessary for practical use of the method, which allows perfectly anisotropic NW growth over a finite χ_{HCl} parameter space and with tolerance to small variations in χ_{HCl}.

The total NW volume decreases continuously with χ_{HCl} (Fig. 2(b)). This indicates that HCl reacts even at these low temperatures with one or several In-based species (TMI, dimethylindium, monomethylindium, and In) and InP, to form InCl, as reported for *in situ* selective area etching [19, 20]. The use of HCl during NW growth makes the process both more complex—possibly involving pre-reactions and depletion of In species—and dynamic, with competing adsorption (growth) and desorption (etching) of growth species. The increasing length for low χ_{HCl} indicates that some of the reaction material contributes to axial growth of the NW, most likely due to diffusion of adsorbed

InCl towards the metal particle/NW growth interface where it contributes to the In supply. The decreasing length for $\chi_{HCl} > 1.5 \times 10^{-5}$ can be interpreted as a depletion of In species, but also as the Au alloy particle being a catalyst for etching of the particle/NW interface, similar to silver particles in HF etching of Si [22]. The two effects may be simultaneously active.

We identify three mechanisms by which the fundamentally interesting and technologically important parameter space giving constant NW diameter and only a change in NW length by increasing χ_{HCl} occur: (1) physisorbed In species are more vulnerable to Cl attack, compared to chemisorbed In situated within the core of the NW formed during axial growth; (2) selectivity of the process due to the original NW side facets having a lower surface free energy than those formed during sidewall growth; (3) desorption of InCl from the NW side facets might be rate limiting, hindering further Cl attack on In species [19]. In order to understand the dynamics of *in situ* NW etching in more detail, additional experiments using *in situ* HCl during and after NW growth are necessary but beyond the scope of this paper.

TEM micrographs displayed in Fig. 3 confirm that the sample grown with $\chi_{HCl} = 3.3 \times 10^{-5}$ has no measurable tapering. Crystal defects arising from twinning on a (111) NW side facet during unintentional radial growth, as pointed out by arrows in Fig. 3(a), were frequently observed during TEM inspection of reference wires. In stark contrast, no such defects were observed during inspection of the non tapered wires. No effect of χ_{HCl} on the Au alloy particles was observed at these temperatures.

Reference NWs ($\chi_{HCl} = 0$, Fig. 3(a)) were observed to consist of almost pure ZB without WZ segments, with the exception of twinning. A gradual change towards a mixture of both WZ and ZB was seen with increasing HCl fraction. For $\chi_{HCl} = 1.0 \times 10^{-5}$ (not shown) and $\chi_{HCl} = 3.3 \times 10^{-5}$ (Fig. 3(c)) the WZ fraction increased to 34% and 55%, respectively. Fourier filtered images (Figs. 3(b) and 3(d)) show the distribution of ZB (red) and WZ (blue) segments in a reference NW, and in an etched ($\chi_{HCl} = 3.3 \times 10^{-5}$) NW, respectively. The reason for the change in crystal structure is not

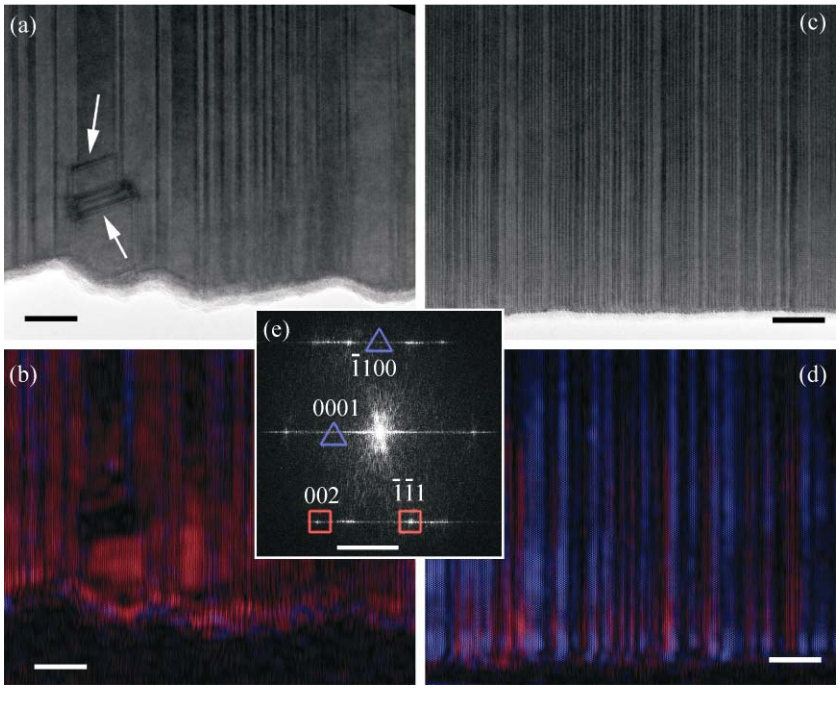

Figure 3 Structural properties of *in situ* etched nanowires. (a) shows the original TEM image and (b) the Fourier filtered image of the reference NW ($\chi_{HCl} = 0$). (c) and (d) show the corresponding images of an InP NW grown using $\chi_{HCl} = 3.3 \times 10^{-5}$. The scale bar is 10 nm. (e) is the fast Fourier transform (FFT) of (a) showing the reflections used to filter out the ZB (squares) and WZ (triangles) polymorphs from (a) and (c) to obtain (b) and (d), respectively. The FFT scale bar is 2 nm^{-1}

clear. Tentatively, we propose that the surface tension between the metal particle and the NW interface is affected by the introduction of HCl, similar to the effect of using diethylzinc during InP NW growth [23]. At this point we cannot quantify to which extent the change in crystal structure with χ_{HCl} affects the dynamic etching/growth behavior.

The low temperature PL spectra of the NWs are shown in Fig. 4. The PL spectra for the reference NWs were registered at 10× the excitation power, necessary for detecting any luminescence. The weak and broad luminescence, below the InP band gap energy (1.42 eV), for the reference NWs is attributed to carbon-related transitions (e.g., via carbon impurities which have a binding energy of about 40 meV [24, 25]), and possibly other defects and impurities.

In contrast, *in situ* etched NWs display a more intense and narrow PL signal, with transitions from 1.38 eV, extruding towards 1.45 eV. Notably, the PL is 20–200 times more intense for etched NWs, even for NWs with an absorption/emission volume of only

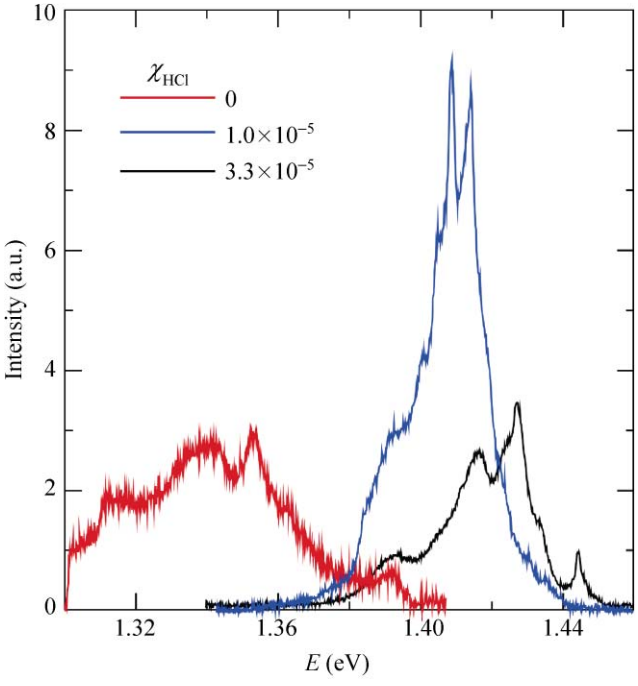

Figure 4 Optical properties of *in situ* etched nanowires. Representative PL spectra taken from wires grown with different $\chi_{HCl} = 0$, 1.0×10^{-5}, and 3.3×10^{-5}. The spectra shown were recorded using an excitation intensity of 6×10^5, 6×10^4, and 6×10^4 W·m^{-2}, respectively

19% of the tapered reference NW. The tendency towards WZ formation when using HCl during growth may result in optical transitions in the energy range 1.38 eV (recombination between WZ and ZB segments [26, 27]), to 1.49 eV (the band gap of WZ InP) [26, 27]. Thus, the transition at 1.38 eV in the optical spectra from *in situ* etched NWs is not necessarily related to carbon impurities. As expected from NWs containing alternating WZ and ZB segments [27], we observed a blue shift of the luminescence in power-dependent measurements (not shown).

We can identify three mechanisms by which *in situ* etching leads to improved optical performance: (1) prevention of shell growth with its structural defects; (2) preferential carbon incorporation via radial (thin film) growth on the NW sidewalls, as recently suggested for GaAs NWs [12] (The Au particle, in which carbon has a low solubility [28] filters out carbon contamination from incorporation into the core of the NW. This effect may be enhanced by the catalytic decomposition of group Ⅲ [29] and group Ⅴ [9] precursors on the Au alloy particle.); (3) Efficient elimination of methyl groups by hydrogen radicals originating from decomposing HCl. This would explain why NWs that still have a shell and are grown with low χ_{HCl} display negligible carbon-related PL signals.

4. Conclusions

We have shown that competitive radial growth in MOVPE of InP NWs can be fully impeded by *in situ* etching. Crystal defects arise during unintentional radial growth occurring at low temperature, and can be removed by use of HCl. A trend towards WZ formation in the NWs is observed with increasing χ_{HCl}. PL spectra demonstrate strongly enhanced optical properties as compared to reference NWs. Our results will allow functionality and performance of NW-based devices to be substantially improved as growth parameters can be chosen for optimal crystal quality rather than optimal morphologic design. The concept of simultaneous etching and growth to induce perfect growth anisotropy may lead to new opportunities for perfection and applications of nanosized materials.

Acknowledgements

This work was performed within the Nanometer Structure Consortium at Lund University and supported by the Swedish Energy Agency, the Swedish Research Council, the Swedish Foundation for Strategic Research, and by the EU programs AMON-RA (No. 214814) and NODE (No. 015783). This report is based on a project which was funded by E.ON AG as part of the E.ON International Research Initiative. Responsibility for the content of this publication lies with the authors.

References

[1] De Franceschi, S.; van Dam, J. A.; Bakkers, E. P. A. M.; Feiner L. F.; Gurevich, L.; Kouwenhoven, L. P. Single-electron tunneling in InP nanowires. *Appl. Phys. Lett.* **2003**, *83*, 344–346.

[2] Bryllert, T.; Wernersson, L. E.; Fröberg, L. E.; Samuelson, L. Vertical high-mobility wrap-gated InAs nanowire transistor. *IEEE Electron. Dev. Lett.* **2006**, *27*, 323–325.

[3] Huang, Y.; Duan, X. F.; Cui, Y.; Lauhon, L. J.; Kim, K. H.; Lieber, C. M. Logic gates and computation from assembled nanowire building blocks. *Science* **2001,** *294,* 1313–1317.

[4] Zheng, G. F.; Patolsky, F.; Cui, Y.; Wang, W. U.; Lieber, C. M. Multiplexed electrical detection of cancer markers with nanowire sensor arrays. *Nat. Biotechnol.* **2005,** *23,* 1294–1301.

[5] Dick, K. A.; Deppert, K.; Larsson, M. W.; Martensson, T.; Seifert, W.; Wallenberg, L. R.; Samuelson, L. Synthesis of branched "nanotrees" by controlled seeding of multiple branching events. *Nat. Mater.* **2004,** *3,* 380–384.

[6] Bakkers, E. P. A. M.; Borgström, M. T.; Verheijen, M. A. Epitaxial growth of Ⅲ–Ⅴ nanowires on group Ⅳ substrates. *MRS Bull.* **2007,** *32,* 117–122.

[7] Regolin, I.; Sudfeld, D.; Luttjohann, S.; Khorenko, V.; Prost, W.; Kastner, J.; Dumpich, G.; Meier, C.; Lorke, A.; Tegude, F. J. Growth and characterisation of GaAs/InGaAs/GaAs nanowhiskers on (111) GaAs. *J. Cryst. Growth* **2007,** *298,* 607–611.

[8] Borgström, M.; Deppert, K.; Samuelson, L.; Seifert, W. Size- and shape-controlled GaAs nano-whiskers grown by MOVPE: A growth study. *J. Cryst. Growth* **2004,** *260,* 18–22.

[9] Verheijen, M. A.; Immink, G.; deSmet, T.; Borgstrom, M. T.; Bakkers, E. P. A. M. Growth kinetics of heterostructured GaP–GaAs nanowires. *J. Am. Chem. Soc.* **2006,** *128,* 1353–1359.

[10] Joyce, H. J.; Gao, Q.; Tan, H. H.; Jagadish, C.; Kim, Y.; Zhang, X.; Guo, Y. N.; Zou, J. Twin-free uniform epitaxial GaAs nanowires grown by a two-temperature process. *Nano. Lett.* **2007,** *7,* 921–926.

[11] Lauhon, L. J.; Gudiksen, M. S.; Wang, C. L.; Lieber, C. M. Epitaxial core–shell and core–multishell nanowire hetero-structures. *Nature* **2002,** *420,* 57–61.

[12] Joyce, H. J.; Gao, Q.; Tan, H. H.; Jagadish, C.; Kim, Y.; Fickenscher, M. A.; Perera, S.; Hoang, T. B.; Smith, L. M.; Jackson, H. E.; Yarrison-Rice, J. M.; Zhang, X.; Zou, J. Unexpected benefits of rapid growth rate for Ⅲ–Ⅴ nanowires. *Nano Lett.* **2009,** *9,* 695–701.

[13] Suhara, M.; Nagao, C.; Honji, H.; Miyamoto, Y.; Furuya, K.; Takemura, R. Atomically flat OMVPE growth of GaInAs and InP observed by AFM for level narrowing in resonant tunneling diodes. *J. Cryst. Growth* **1997,** *179,* 18–25.

[14] Stringfellow, G. B. *Organometallic Vapor Phase Epitaxy: Theory and Practice*, 2nd edn; Academic Press: San Diego, 1999.

[15] Chen, C. H.; Kitamura, M.; Cohen, R. M.; Stringfellow, G. B. Growth of ultrapure InP by atmospheric-pressure organometallic vapor-phase epitaxy. *Appl. Phys. Lett*. **1986,** *49,* 963–965.

[16] Hsu, C. C.; Yuan, J. S.; Cohen, R. M.; Stringfellow, G. B. Doping studies for InP grown by organometallic vapor-phase epitaxy. *J. Cryst. Growth* **1986,** *74,* 535–542.

[17] Dick, K. A.; Deppert, K.; Samuelson, L.; Seifert, W. InAs nanowires grown by MOVPE. *J. Cryst. Growth* **2007,** *298,* 631–634.

[18] Dayeh, S. A.; Yu, E. T.; Wang, D. Ⅲ–Ⅴ nanowire growth mechanism: Ⅴ/Ⅲ ratio and temperature effects. *Nano Lett.* **2007,** *7,* 2486–2490.

[19] Caneau, C.; Bhat, R.; Koza, M.; Hayes, J. R.; Esagui, R. Etching of InP by HCl in an OMVPE Reactor. *J. Cryst. Growth* **1991,** *107,* 203–208.

[20] Kitatani, T.; Tsuchiya, T.; Shinoda, K.; Aoki, M. *In situ* etching of InGaAsP/InP by using HCl in an MOVPE reactor. *J. Cryst. Growth* **2005,** *274,* 372–378.

[21] Magnusson, M. H.; Deppert, K.; Malm, J. O.; Bovin, J. O.; Samuelson, L. Size-selected gold nanoparticles by aerosol technology. *Nanostruct. Mater.* **1999,** *12,* 45–48.

[22] Tsujino, K.; Matsumura, M. Morphology of nanoholes formed in silicon by wet etching in solutions containing HF and H_2O_2 at different concentrations using silver nanoparticles as catalysts. *Electrochim. Acta* **2007,** *53,* 28–34.

[23] Algra, R.; Verheijen, M. A.; Borgström, M. T.; Feiner, L. F.; Immink, G.; van Enckevort, W. J. P.; Vlieg, E.; Bakkers, E. P. A. M. Twinning superlattices in indium phosphide nanowires. *Nature* **2008,** *456,* 369–372.

[24] Skromme, B. J.; Stillman, G. E.; Oberstar, J. D.; Chan, S. S. Photoluminescence identification of the C and Be acceptor levels in InP. *J. Electron. Mater.* **1984,** *13,* 463–491.

[25] Fry, K. L.; Kuo, C. P.; Larsen, C. A.; Cohen, R. M.; Stringfellow, G. B.; Melas, A. OMVPE Growth of InP and $Ga_{0.47}In_{0.53}As$ using ethyldimethylindium. *J. Electron. Mater.* **1986,** *15,* 91–96.

[26] Pemasiri, K.; Montazeri, M.; Gass, R.; Smith, L. M.; Jackson, H. E.; Yarrison-Rice, J.; Paiman, S.; Gao, Q.; Tan, H. H.; Jagadish, C.; Zhang, X.; Zou, J. Carrier dynamics and quantum confinement in type Ⅱ ZB–WZ InP nanowire homostructures. *Nano Lett.* **2009,** *9*, 648–654.

[27] Bao, J. M.; Bell, D. C.; Capasso, F.; Wagner, J. B.; Martensson, T.; Tragardh, J.; Samuelson, L. Optical properties of rotationally twinned InP nanowire heterostructures. *Nano Lett.* **2008,** *8*, 836–841.

[28] Okamoto, H.; Massalski, T. B. The Au–C (gold-carbon) system. *J. Phase Equil.* **1984,** *5*, 378–379.

[29] Borgström, M. T.; Immink, G.; Ketelaars, B.; Algra, R.; Bakkers, E. P. A. M. Synergetic nanowire growth. *Nat. Nanotechnol.* **2007,** *2*, 541–544.